

Wouter J. H. Veldkamp  
Lucia J. M. Kroft  
Mireille V. Boot  
Bart J. A. Mertens  
Jacob Geleijns

## Contrast-detail evaluation and dose assessment of eight digital chest radiography systems in clinical practice

Received: 1 March 2005  
Revised: 27 June 2005  
Accepted: 29 July 2005  
Published online: 31 August 2005  
© Springer-Verlag 2005

W. J. H. Veldkamp · L. J. M. Kroft ·  
M. V. Boot · J. Geleijns  
Department of Radiology, C2S,  
Leiden University Medical Center,  
Albinusdreef 2,  
2333 ZA Leiden, The Netherlands

B. J. A. Mertens  
Department of Medical Statistics, C2S,  
Leiden University Medical Center,  
Albinusdreef 2,  
2333 ZA Leiden, The Netherlands

W. J. H. Veldkamp (✉)  
Department of Radiology, C2S,  
Leiden University Medical Center,  
PO Box 9600, 2300 RC Leiden,  
The Netherlands  
e-mail: w.j.h.veldkamp@lumc.nl  
Tel.: +31-71-5263689  
Fax: +31-71-5248256

**Abstract** The purpose of this study was to assess contrast-detail performance and effective dose of eight different digital chest radiography systems. Digital chest radiography systems from different manufacturers were included: one storage phosphor system, one selenium-coated drum system, and six direct readout systems including four thin-film transistor (TFT) systems and two charge-coupled device (CCD) systems. For measuring image quality, a contrast-detail test object was used in combination with a phantom that simulates the primary and scatter transmission through lung fields (LucAl). Six observers judged phantom images of each modality by soft-copy reading in a four-alternative-forced-choice experiment. The entrance dose was also measured, and the effective dose was calculated for an average patient.

Contrast-detail curves were constructed from the observer data. The blocked two-way ANOVA test was used for statistical analysis. Significant difference in contrast-detail performance was found between the systems. Best contrast-detail performance was shown by a CCD system with slot-scan technology, and the selenium-coated drum system was compared to the other six systems ( $p$  values  $\leq 0.003$ ). Calculated effective dose varied between 0.010 mSv and 0.032 mSv. Significant differences in contrast-detail performance and effective dose levels were found between different digital chest radiography systems in clinical practice.

**Keywords** Digital radiography · Flat-panel detector · Chest radiography

### Introduction

In the last decade, several digital chest radiography technologies have been developed. Various systems have become commercially available and are now used in clinical practice. A major difference between these systems concerns the methods used to capture the X-ray image, i.e., differences in detector technology. These technical differences may have their influence on image quality, such as contrast-detail performance.

With computed radiography (CR), the cassette containing a photostimulable storage phosphor plate with the captured X-ray exposure pattern is placed in a reader after exposure. The latent image is read using laser-stimulated

light emission of electrons trapped in the phosphor valence bands during X-ray exposure. Signals are digitized and stored in a computer [1].

Another system used for digital chest imaging uses a selenium-coated drum as detector and microelectrometers for readout [2, 3]. For scatter reduction, an air gap instead of an antiscatter grid is used in the system.

Digital direct readout radiography (DR) systems can be grouped into systems with direct conversion detectors and systems with indirect conversion detectors. With direct conversion detectors, amorphous selenium (Se) is used as the semiconductor material to convert the X-ray photons into electric charge immediately. Before exposure, an electric field is applied across the amorphous Se layer

through a bias electrode on the top surface of the Se layer. As X-rays are absorbed in the detector, electric charges are freed and drawn to collecting electrodes. The collected charges are read out by thin-film transistors (TFTs) and then converted into a digital image. This is the case in the Se flat-panel detectors (Se-FPD). With indirect conversion detectors, a scintillator is used to convert the X-rays into visible light. Gadolinium oxide sulfide (GOS) or cesium iodide (CsI) layers are used as scintillators to capture the X-ray energy for chest radiography. The visible light is then converted into charge by a matrix of silicon photodiodes (scintillator FPD systems) or by charge-coupled devices (CCDs). The signals are read out by TFTs and converted to a digital image.

Essential technical differences exist among the various digital chest systems currently on the market. However, little is known about how these differences may reflect in terms of image quality. Contrast-detail studies provide key information of image quality [4]. The purpose of this study was to assess the contrast-detail performance and effective

dose of eight different digital radiography systems that are presently in use for routine clinical chest radiography.

## Materials and methods

The following systems were included in the study: two indirect conversion CsI-FPDs, two indirect conversion CCD systems (one lens coupled and one slot scan), one indirect conversion GOS-FPD, one direct conversion Se-FPD, one CR system, and one Se-coated drum system. System information and technical characteristics are given in Table 1 [1]. The eight systems were located in six separate hospitals in the Netherlands.

### Contrast-detail object

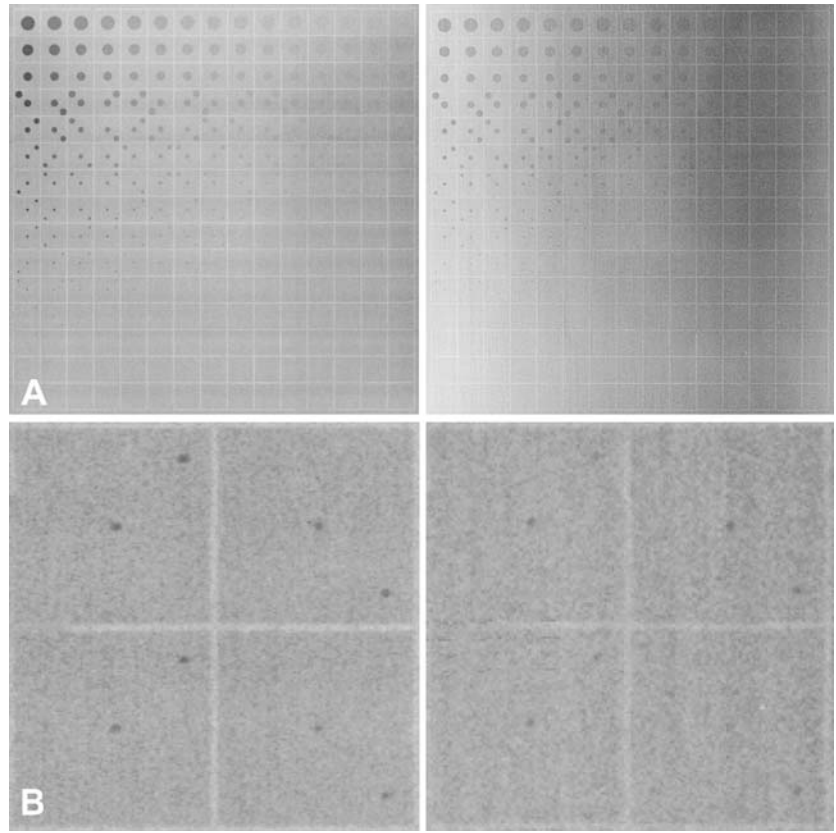
The contrast-detail test object (CDRAD; University Medical Center Nijmegen, Nijmegen, The Netherlands) was

**Table 1** Technical data for each chest system

System type (detector)	CsI-FPD-1	CsI-FPD-2	Lens-coupled CCD	Slot-scan CCD	GOS-FPD	Se-FPD	CR	Se-drum
Company	Siemens	Philips	Swissray	Delft Imaging Systems	Canon	Tromp Medical Engenering	Fuji	Philips
Product name	Thorax FD	Digital Diagnost	ddR Combi-System	Thorascan	CXDI 40G	DR 1000C	Fuji storage phosphor <sup>a</sup>	Thoravision
Detector material	Scintillator	Scintillator	Scintillator	Scintillator	Scintillator	Photoconductor	Storage phosphor	Photoconductor
System type (chest stand or general purpose)	Chest/skeletal	General	General	Chest	General	Chest	Chest/skeletal	Chest
Pixel size/detector elements (µm)	143	143	167	162	160	139	200	200
Focus to image plane distance (cm)	180	200	200	183	202	180	200	200
Scatter reduction (slit or grid)	Grid	Grid	Grid	Slit	Grid	Grid	Grid	Airgap
Detector material	Cesium iodine	Cesium iodine	Cesium iodine	Cesium iodine	GOS (Gd2O2S)	Selenium	Barium fluoride	Selenium
Conversion to electrical charge	Photodiode	Photodiode	CCD	CCD	Photodiode	Photoconductor	Photomultiplier	Scanning microelectrometers

<sup>a</sup>Multix Bucky system (Siemens) with FCR 5000 R reader (Fuji) and image plate ST-Vn  
*CsI-FDP* cesium iodine flat-panel detector, *CCD* charge-coupled device, *GOS-FPD* gadolinium oxide sulfide flat-panel detector, *Se-FPD* selenium flat-panel detector, *CR* computed radiography, *Se-drum* selenium-coated drum system

**Fig. 1 a** Radiographic representation of the contrast-detail test object (CDRAD) using the slot-scan charge-coupled device (CCD) system (*left image*) and the computed radiography (CR) system (*right image*). Window width and window level were adjusted to obtain comparable presentation of the images with respect to object contrast and background intensity. Note the differences in image homogeneity between the systems.  
**b** Two fragments of the CDRAD object containing dots of 0.6 and 0.5 mm are shown. The dots appear clearer in the *left image* that corresponds to the slot-scan CCD system. The *right image* corresponds to the CR system



applied to investigate contrast-detail performance. This object is a polymethyl methacrylate (PMMA) plate with a thickness of 1 cm and an area of 26.5×26.5 cm. A matrix on the plate of 15×15 squared cells contains holes of varying size and depth. In the first three rows of the matrix, each cell contains one central hole [5]. The remaining cells in the matrix contain one central hole and one hole in one of the four corners. Hole diameter varies in horizontal direction (logarithmically from 0.3 to 8 mm) whereas hole depth varies in vertical direction (logarithmically from 0.3 to 8 mm). Figure 1 gives radiographic representations of the phantom using two different digital chest radiography systems.

#### Image acquisition

The CDRAD object was placed in a LucAl phantom [6]. This phantom simulates lung transmission characteristics and is constructed from slabs of polymethylmethacrylate (PMMA) and aluminum. It includes a 19 cm air gap. The CDRAD object was placed halfway in the air gap. Six images were acquired with the described configuration with each digital chest system in the corresponding hospital, resulting in 48 images. Acquiring six images at each system reduces the influence of the accidental quantum noise

distribution over the image and hence its effect on the contrast-detail performance.

The clinical protocols of the systems assessed in this study were established by recommendations of the manufacturers and customized by physicists and radiologists. This reflects good clinical practice. The same tube voltage (kV) as in clinical practice was used. The tube charge (mAs) was determined by automatic exposure control (AEC) (Table 2). Standard postprocessing as usual in clinical practice was applied to the images for each system, as is usual in clinical practice. For optimizing the image quality for each individual digital radiography system, the following method was used: for each individual system, the window level was taken equal to the mean pixel value in the CDRAD images. The window width was determined for each individual system by histogram analysis of images of an anthropomorphic chest phantom representing a standardized adult patient (Model PBU-S-3, Kaguka Company, Kyoto, Japan). The histogram was determined in a predefined squared region containing the lung and mediastinal area of the phantom but no image background. The outer 1% sides of the histogram were excluded. The window width was taken equal to the remaining 98% histogram width. For detecting the holes, it would have been advantageous to choose a very small window width since the image background is uniform. However, using such a small window width is not clinically relevant.

**Table 2** Calculated patient dose for posteroanterior chest images and corresponding parameter settings

Modality	Tube voltage (kV)	Total filtration (mm Al eq.+mm Cu)	Tube charge (mAs)	Entrance surface dose ( $\mu\text{Gy}$ ) <sup>a</sup>	Effective dose (mSv) <sup>b</sup>
CsI-FPD-1	125	0.1 Cu	1.0	33	0.010
CsI-FPD-2	150	1.0 Al+0.1 Cu	0.8	35	0.011
Lens-coupled CCD	125	2.5 Al+0.1 Cu	1.7	58	0.017
Slot-scan CCD	133	3.0 Al+0.3 Cu	61.3	54	0.020
GOS-FPD	141	0.9 Al+0.3 Al	1.6	91	0.021
Se-FPD	125	2.5 Al+0.1 Cu	2	80	0.024
CR	125	3.0 Al	– <sup>c</sup>	109	0.028
Se-drum	150	1.0 Al+0.2 Cu	2.5	98	0.032

<sup>a</sup>Entrance skin dose (excluding backscatter) was measured on the LucAl phantom

<sup>b</sup>Effective doses are calculated for an average patient

<sup>c</sup>For the CR system, the mAs value was not indicated by the system

CsI-FPD cesium iodine flat-panel detector, CCD charge-coupled device, GOS-FPD gadolinium oxide sulfide flat-panel detector, Se-FPD selenium flat-panel detector, CR computed radiography, Se-drum selenium-coated drum system

### Image reading

Soft-copy image reading was done from one and the same Dome C3 1,536×2,048 pixel grey scale flat panel (Dome Imaging Systems, Inc. Waltham, MA, USA). The monitor complied with the requirements of the American Association of Physicists in Medicine (AAPM) [7]. The monitor had a maximum luminance of 690 Cd/m<sup>2</sup>.

Only slightly better contrast-detail performance was reported with 2 K than with 1 K monitors in full-screen display mode [8]. For this comparative study, the pixel matrix size of the monitor used is not expected to be a limiting factor. Moreover, in this study, the images were presented larger than full-screen mode.

Six observers performed image reading: three physicists, one quality assurance technician, one radiologist, and one physics student. Each observer scored two images per system. The order in which the different imaging systems were scored was randomized to exclude the influence of a learning effect.

The images were displayed using eFilm (eFilm Medical Inc., Toronto, Canada) and magnified by a factor 1.5 to limit the influence of pixel matrix size, as explained above. This factor was a compromise, as applying a larger magnification would increase the need for roaming and thereby the scoring time. The images were made anonymous in such way that the radiography system could not be recognized on the image. Roaming was used to evaluate the entire CDRAD image. It was not allowed to use other soft-copy tools (such as window width and window level). The observers were free to choose their viewing distance. Care was taken to ensure standard and optimal environmental light conditions.

The first three rows of the CDRAD matrix images, with cells containing only a central dot, were not included in the evaluation. With respect to the remaining cells, a four-alternative-forced-choice detectability (4-AFC) experiment was performed: the observers were asked to indicate the

dot-containing corner in each cell. Even when dots could not be detected, the observers were instructed to make a decision. A paper template and a pencil were used to indicate the dot's location. Observers were free to define their time schedule for scoring the eight systems, but they were instructed to interrupt a session after scoring two systems.

### Radiation exposure

During image acquisition of the CDRAD object, entrance surface dose was measured on the LucAL phantom using a Wellhöfer dosimeter WD10 (Wellhöfer Dosimetrie, Schwarzenbruck, Germany). The mean entrance skin dose was determined from the six exposures for each system. PCXMC software was used for calculating the effective dose for an average adult patient (height 174 cm; weight 71.1 kg) [9]. This computer program is based on Monte Carlo simulation and it allows a free choice of projection geometry, X-ray spectrum, and patient size.

### Data analysis

A reference template was used for evaluation of the annotated template papers. An interpolation method was used to determine the detection probability for each cell [10]. This was derived from the scoring results of the six observers. For each hole diameter, a hole depth detection threshold was calculated that corresponds with 62.5 % correct responses. This is just in the middle of the detection probability range that runs from 25% to 100%. A second-order polynomial fit was used to finally fit a contrast-detail curve through the threshold hole depth values.

Statistical analysis of contrast-detail results was done using blocked two-way ANOVA with S-PLUS software (Insightful Corporation, Seattle, WA, USA). The two in-

dependent variables were machine type and hole diameter, and the dependent variable was threshold hole depth. First, the null hypothesis that threshold depth values of the different systems come from populations with the same means was tested. Since this null hypothesis could be rejected, multiple comparisons of all 28 possible pairs of different systems were made. For critical-point calculation, the Bonferroni method was used.

## Results

The 4-AFC-experiment detection curves that were fitted through the threshold hole depth values are shown in Fig. 2. Blocked two-way ANOVA indicated a strong statistically significant difference in contrast-detail performance between the eight digital radiography systems ( $p$  value= $1.1 \cdot 10^{-12}$ ;  $F=20.8$ ; degrees of freedom=7).

The multiple comparison contrast-detail results for all systems are given in Table 3. No statistical difference was found in the contrast-detail threshold values between the slot-scan CCD system and the Se-coated drum system. The threshold values and the fitted curves of the two systems were statistically significantly lower than those of the other six systems, with consequently better contrast-detail performance ( $p$  values all  $\leq 0.003$ ). No significant differences were found between the six remaining systems, except for slightly worse contrast-detail performance that was found with the CR system as compared with the lens-coupled CCD system.

## Radiation exposure

In Table 2, the entrance dose levels and calculated effective dose levels are given. A large variation was found

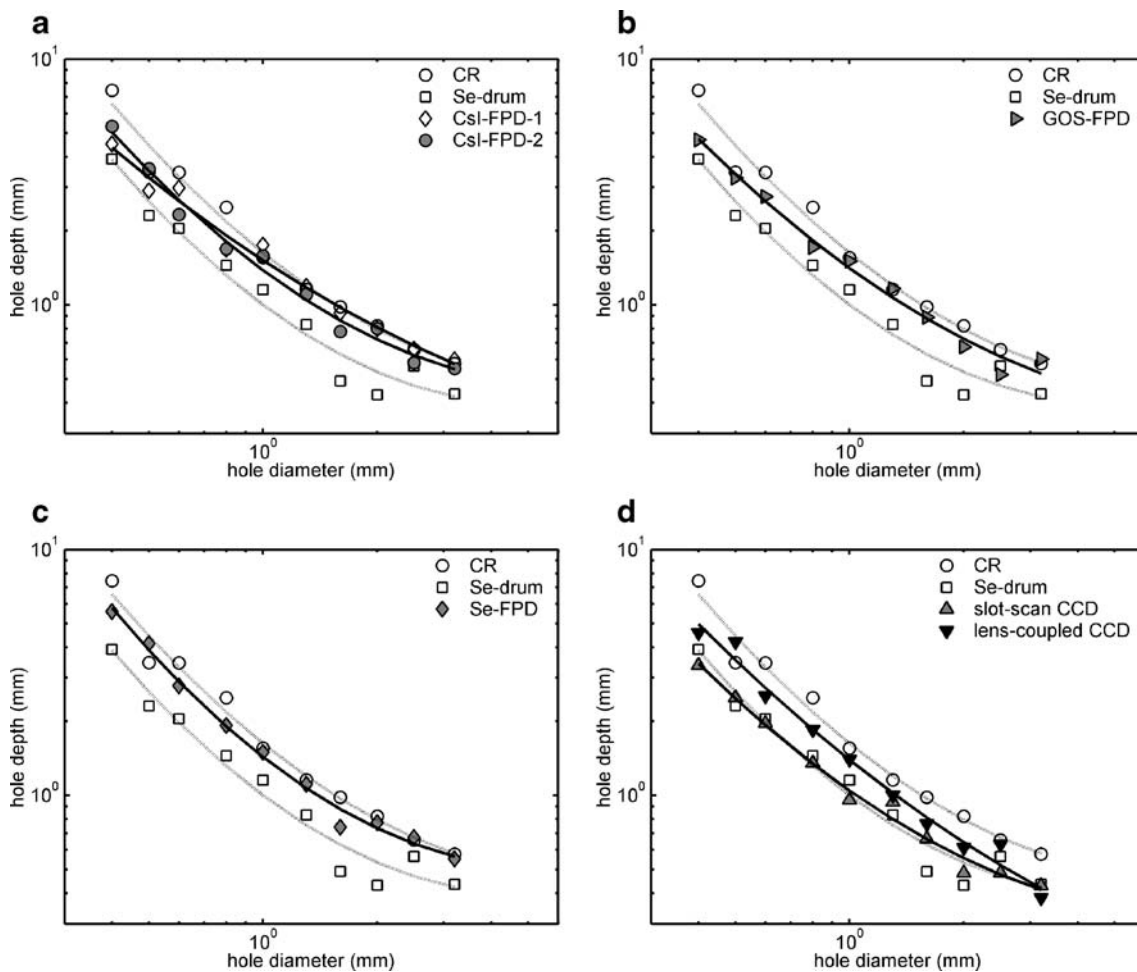


**Fig. 2** Contrast-detail curves of the eight different digital radiography systems. The curves are fitted through 62.5% threshold values for contrast-detail observations. Each curve represents data for all six observers. Curves of cesium iodine flat-panel detector (CsI-FPD)-1 and CsI-FPD-2 (a), gadolinium oxide sulfide flat-panel detector

(GOS-PPD) (b), selenium flat-panel detector (Se-PPD) (c), and slot-scan charge-coupled device (CCD) and lens-coupled CCD (d) are shown. Curves of computed radiography (CR) and selenium-coated drum system (Se-drum) are shown in each figure as a reference

**Table 3** Systems are compared pair-wise based on the detection threshold depth values for each

	Estimate <sup>a</sup>	Lower bound <sup>a</sup>	Upper bound <sup>a</sup>	<i>P</i> value <sup>a</sup>
Slot-scan CCD-CsI-FPD-1	-0.15000	-0.22900	-0.0703	0.000
Slot-scan CCD-CR	-0.21300	-0.29200	-0.1330	0.000
Slot-scan CCD-lens-coupled CCD	-0.12100	-0.20000	-0.0415	0.003
Slot-scan CCD-GOS-FPD	-0.13500	-0.21400	-0.0553	0.001
Slot-scan CCD-Se-FPD	-0.15800	-0.23700	-0.0784	0.000
Slot-scan CCD-Se-drum	0.00925	-0.07020	0.0887	0.819
Slot-scan CCD-CsI-FPD-2	-0.13800	-0.21700	-0.0585	0.001
CsI-FPD-1-CR	-0.06280	-0.14200	0.0167	0.121
CsI-FPD-1-lens-coupled CCD	0.02890	-0.05060	0.1080	0.475
CsI-FPD-1-GOS-FPD	0.01510	-0.06440	0.0945	0.710
CsI-FPD-1-Se-FPD	-0.00807	-0.08750	0.0714	0.842
CsI-FPD-1-Se-drum	0.15900	0.07960	0.2390	0.000
CsI-FPD-1-CsI-FPD-2	0.01190	-0.06760	0.0914	0.769
CR-lens-coupled CCD	0.09170	0.01220	0.1710	0.024
CR-GOS-FPD	0.07780	-0.00163	0.1570	0.055
CR-Se-FPD	0.05470	-0.02480	0.1340	0.177
CR-Se-drum	0.22200	0.14200	0.3010	0.000
CR-CsI-FPD-2	0.07470	-0.00481	0.1540	0.065
Lens-coupled CCD-GOS-FPD	-0.01380	-0.09330	0.0657	0.734
Lens-coupled CCD-Se-FPD	-0.03690	-0.11600	0.0425	0.361
Lens-coupled CCD-Se-drum	0.13000	0.05070	0.2100	0.001
Lens-coupled CCD-CsI-FPD-2	-0.01700	-0.09650	0.0625	0.675
GOS-FPD-Se-FPD	-0.02310	-0.10300	0.0563	0.570
GOS-FPD-Se-drum	0.14400	0.06450	0.2230	0.000
GOS-FPD-CsI-FPD-2	-0.00318	-0.08260	0.0763	0.937
Se-FPD-Se-drum	0.16700	0.08770	0.2470	0.000
Se-FPD-CsI-FPD-2	0.02000	-0.05950	0.0994	0.622
Se-drum-CsI-FPD-2	-0.14700	-0.22700	-0.0677	0.000

<sup>a</sup>Estimates, *p* values and 95% confidence intervals (lower bound, upper bound) of the blocked two-way ANOVA test are given. To adjust for multiple comparisons, critical point calculation was based on the Bonferroni method. A negative estimate indicates a lower (better) contrast-detail curve for the first system in each comparison. Confidence intervals excluding zero indicate significant difference between systems ( $p < 0.05$ ). The standard error was 0.0241 for all comparisons

CCD charge-coupled device, CsI cesium iodine; FDP flat-panel detector, CR computed radiography, GOS gadolinium oxide sulfide, Se selenium, Se-drum selenium-coated drum system

in entrance dose and thereby in effective dose levels between the systems. The Se-coated drum system was related to the highest effective dose level in this study. Effective dose of the slot-scan CCD took a middle position in the spectrum. The effective dose levels for the two CsI-FPD systems were roughly a factor 2 lower as compared with the other systems. Figure 3 shows the image quality for each system together with the calculated effective dose for each system. Between the systems, no direct relationship was found between image quality and calculated effective dose.

## Discussion

In a short period, various digital radiography chest systems have been implemented in clinical practice. We have

investigated the image quality—expressed as contrast-detail performance—of different digital radiography systems in the range of digital chest systems that are nowadays available: CR, Se-coated drum, FPDs, and CCD-based systems. The starting point of the study was that the acquisitions for each system used were the same as for imaging patients in usual clinical practice. As a consequence, good clinical imaging quality for each system was assumed. This study shows significant differences in contrast-detail performance between various digital imaging systems implemented in clinical practice. In addition, the calculated effective doses varied between these systems. The overall difference found in image quality between the various systems was not directly related to the variation in dose between the systems. Hence, system dose alone cannot sufficiently explain the differences in image quality. An additional explanation should lie in other parts of the digital radiography chain,

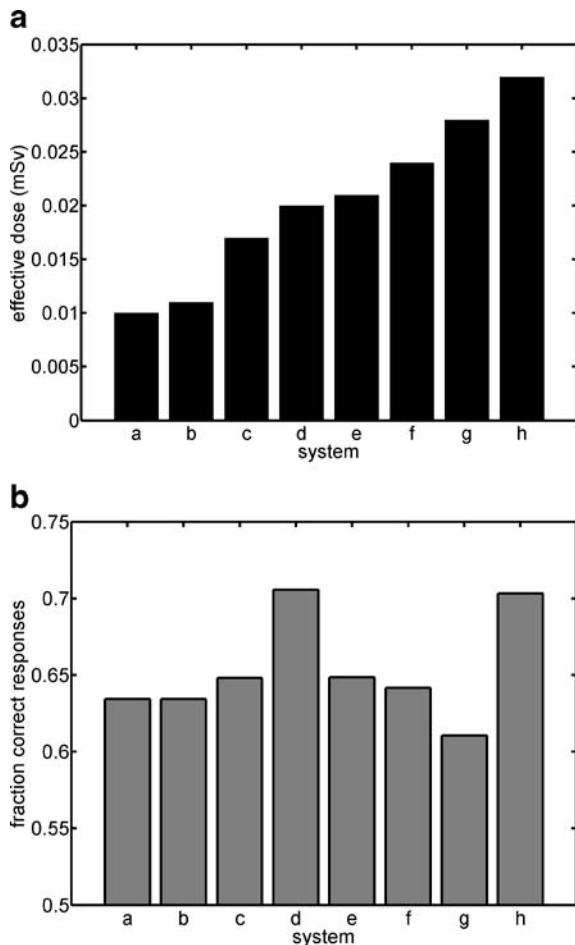


**Fig. 3** **a** Effective dose for *a* cesium iodine flat-panel detector (CsI-FPD-1), *b* CsI-FPD-2, *c* lens-coupled charge-coupled device (CCD), *d* slot-scan CCD, *e*, gadolinium oxide sulfide flat-panel detector (GOS-FPD), *f* selenium flat-panel detector (Se-FPD), *g* computed radiography (CR) and *h* selenium-coated drum system (Se-drum) is shown. **b** Image quality expressed as the fraction correctly detected dots for each system with respect to all 180 observed cells in the contrast-detail test object (CDRAD) averaged over all observations. Note that there is no general trend in relative contrast-detail performance and effective dose level

such as the method for scatter reduction and detector system design.

There were two digital systems with superior contrast-detail performance compared with the other digital systems. These were the recently introduced slot-scan CCD system and the older, well-known, Se-coated drum system. A notable similarity between these systems is that no grid is used for imaging. In general, scatter radiation reaching the detector increases quantum noise in the image without adding useful signal, which deteriorates the SNR relative to the patient dose. Using a grid eliminates most of the scatter but also absorbs part of the primary radiation. When a slot-scan method is used instead of a grid, more of the primary transmitted signal reaches the detector, with comparable low scatter fraction and an improved SNR quality [11, 12]. For

the slot-scan CCD system with CsI detector, better image quality has been shown as compared with conventional screen-film chest radiography [13, 14]. In a recent comparison between eight different digital chest radiography systems, highest detectability of simulated lesions was found with slot-scan CCD [15]. An evaluation of the fundamental imaging characteristics of the slot-scan CCD system showed low scatter fractions and related high image quality [11].

With the Se-coated drum system, an air gap is used instead of a grid; subtle pulmonary lesions are better detected with an air gap than with a grid at the same exposure level [16]. Accordingly, the difference we found in image quality between the Se-FPD system and Se-drum system (both contain a 0.5 mm Se layer [17, 18]) might be explained by the advantage of the air gap used with the Se-drum system as compared with the grid used in the Se-FPD system. In addition, the dose found with the Se-FPD system was slightly lower (about two thirds) than with the Se-drum system. This may have contributed as a limiting factor for contrast-detail performance in the Se-FPD system as well.

Several studies have shown equal or better imaging quality for Se-FPDs compared with storage phosphor systems [19, 20]. In addition, studies have shown superior image quality for the Se-coated drum system compared with storage phosphor systems [17, 21, 22]. The predominantly better image quality for Selenium-based systems is attributed to the relative low detector noise and very high spatial resolution compared with CR [17, 18]. Also, in the current study, the Se-based system's contrast-detail curves were under the curve of the CR system although the difference between Se-FPD and CR was not significant under these clinical conditions. Studies that use physical parameters to investigate image quality as a function of spatial frequency find better performance at low spatial frequencies for CsI-FPD systems than for Se-FPD systems. This is explained by the high atomic number and high density of CsI. On the contrary, the Se-based systems show better performance at the higher spatial frequencies since these systems are superior in spatial resolution [18, 23]. Hence, a univocal difference in contrast-detail performance between CsI-FPD and Se-FPD is not expected. Accordingly, no significant difference was found this study. Here, it must be noted that the effective dose with the Se-FPD system was roughly two times higher than the dose with the CsI-FPD systems.

For indirect conversion detectors, CsI has proved the superior scintillator material. In addition to the high atomic number and high density of CsI, the needle-like structure of CsI strongly reduces the spreading of light in the scintillator that allows the use of a thicker layer with higher efficiency compared with unstructured scintillators [1, 23–25]. Due to the high efficiency of CsI, lower dose levels are recommended with CsI-FPD systems than with screen-film systems [26]. Both the slot-scan CCD system and the lens-coupled CCD systems use CsI as scintillator. The doses used

with these systems were comparable, but a significant difference in contrast-detail performance was found in favor of the slot-scan CCD system. This can be explained by the demagnification process that results in low optical coupling efficiency for the lens-coupled CCD system, with a resulting lower imaging quality [1, 2, 27]. Furthermore, the lens-coupled CCD system uses a grid, which is not needed in the slot-scan CCD system, as has been discussed.

Although better results were found with the CsI slot-scan CCD system, we found no differences in contrast-detail results for the CsI-FPDs as compared with the other scintillator-based GOS and storage-phosphor systems. GOS is an unstructured granular material. Visible light emitted in such material may spread to adjacent pixels, thereby reducing spatial resolution and image quality [1]. In CR, image quality is deteriorated by internally generated noise in these systems, i.e., luminescence and granularity noise [1, 2]. Superior image quality for CsI-FPD systems compared with GOS-FPD and CR could have been expected and has been reported in a number of studies [24, 28–30]. However, in the present study, the effective dose found for the CsI-FPD systems was at least a factor 2 lower than with the other systems. This lower dose may have been insufficient for optimal contrast-detail performance in the CsI-FPD systems.

#### Study limitations

In the present study, differences in contrast-detail performance found between the digital radiography systems have been primarily explained by their system design, as dose alone could not clarify the differences found. Nevertheless, postprocessing methods may also comprise substantial in-

fluence on system performance [31, 32]. We tried to limit these effects by optimizing the window-width and window-level settings for each system and by not allowing postprocessing handlings (other than roaming) by the observers during image reading. Yet, possible specific postprocessing methods (such as MUSICA or other typical system postprocessing techniques developed by the manufacturers) were not manipulated nor evaluated in the present study.

Contrast-detail studies provide important information of image quality. However, a CDRAD object provides a limited representation of clinical images because of lack of anatomical noise in these images. Quantum noise and thus dose level may play a more central role in contrast-detail studies than in clinical studies with patients or anthropomorphic phantoms [33]. More data are needed to precisely determine the effect of difference in contrast-detail performance between various digital radiography systems for imaging patients in clinical practice.

The eight different digital radiography systems were not compared with identical systems settings (e.g., mAs and kV), as the starting point of the study was evaluating these systems as used in clinical practice. Furthermore, the systems have been optimized in different institutions. As a result, the contrast-detail performance may have been affected by suboptimal system settings although it should be noted that strategies for optimal parameter settings for digital systems have not been determined yet. Possible influences of parameter settings for the individual systems used were therefore beyond the scope of the present study.

**Acknowledgements** The authors gratefully acknowledge the participation of the following persons in the panel of observers: J.P. van Delft, V. Schembri MSc, and D. Zweers BSc (Leiden University Medical Center, Department of Radiology).

#### References

1. Kotter E, Langer M (2002) Digital radiography with large-area flat-panel detectors. *Eur Radiol* 12:2562–2570
2. Schaefer-Prokop C, Uffmann M, Eisenhuber E, Prokop M (2003) Digital radiography of the chest: detector techniques and performance parameters. *J Thorac Imaging* 18:124–137
3. Huda W, Slone R. Review of radiologic physics 1995 Lippincott Williams & Wilkins, USA
4. International Commission on Radiation Units and Measurements (1996) Medical imaging—the assessment of image quality. ICRU Report no. 54 Bethesda, Md: International Commission on Radiation Units and Measurements, p. 54
5. Thijssen MA, Thijssen HO, Merx JL, van Woensel MP (1988) Quality analysis of DSA equipment. *Neuroradiology* 30:561–568
6. Conway BJ, Butler PF, Duff JE et al (1984) Beam quality independent attenuation phantom for estimating patient exposure from x-ray automatic exposure controlled chest examinations. *Med Phys* 11:827–832
7. AAPM Report No. 73, American Association of Physicists in Medicine, Quality Control in Diagnostic Radiology (2002) Diagnostic X-ray Imaging Committee Task Group No. 12, July 2002
8. Peer S, Giacomuzzi SM, Peer R, Gassner E, Steingruber I, Jaschke W (2003) Resolution requirements for monitor viewing of digital flat-panel detector radiographs: a contrast detail analysis. *Eur Radiol* 13:413–417
9. Servomaa A, Tapoivaara M (1998) Organ dose calculation in medical x-ray examinations by the program PCXMC. *Radiat Prot Dosim* 80:213–219
10. Veldkamp WJ, Thijssen MA, Karssmeijer N (2003) The value of scatter removal by a grid in full field digital mammography. *Med Phys* 30:1712–1718
11. Samei E, Saunders RS, Lo JY, Dobbins JT III, Jesneck JL, Floyd CE, Ravin CE (2004) Fundamental imaging characteristics of a slot-scan digital chest radiographic system. *Med Phys* 31:1298–2687
12. Diekmann F, Diekmann S, Richter K, Bick U, Fischer T, Lawaczeck R, Press WR, Schon K, Weinmann HJ, Arkadiev V, Bjeoumikhov A, Langhoff N, Rabe J, Roth P, Tilgner J, Wedell R, Krumrey M, Linke U, Ulm G, Hamm B (2004) Near monochromatic X-rays for digital slot-scan mammography: initial findings. *Eur Radiol* 14:1641–1646



13. Veldkamp WJ, Kroft LJ, Mertens BJ, Geleijns J (2005) Comparison of image quality between a digital slot-scan CCD chest radiography system and AMBER and Bucky screen-film radiography chest systems. *Radiology* 235:857–866
14. Kroft LJ, Geleijns J, Mertens BJ, Veldkamp WJ, Zonderland HM, de Roos A (2004) Digital slot-scan charged coupled device chest radiography versus AMBER and Bucky screen-film radiography: detection of simulated chest nodules and interstitial disease using a chest phantom. *Radiology* 231:156–163
15. Kroft LJ, Veldkamp WJ, Mertens BJ, Boot MV, Geleijns J. Comparison of eight digital chest radiography systems: variation in detection of simulated chest disease. *Am J Roentgenol* 185:339–346
16. Bernhardt TM, Rapp-Bernhardt U, Hausmann T, Reichel G, Krause UW, Doehring W (2000) Digital selenium radiography: anti-scatter grid for chest radiography in a clinical study. *Br J Radiol* 73:963–968
17. Neitzel U, Maack I, Gunther-Kohfahl S (1994) Image quality of a digital chest radiography system based on a selenium detector. *Med Phys* 21:509–516
18. Samei E, Flynn MJ (2003) An experimental comparison of detector performance for direct and indirect digital radiography systems. *Med Phys* 30:608–622
19. Awai K, Komi M, Hori S (2001) Selenium-based digital radiography versus high-resolution storage phosphor radiography in the detection of solitary pulmonary nodules without calcification: receiver operating characteristic curve analysis. *Am J Roentgenol* 177:1141–1144
20. Goo JM, Im J-G, Kim JH, et al (2000) Digital chest radiography with selenium-based flat-panel detector versus a storage phosphor system: comparison of soft-copy images. *Am J Roentgenol* 175:1013–1018
21. Mansson LG, Kheddache S, Lanhede B, Tylén U (1999) Image quality for five modern chest radiography techniques: a modified FROC study with an anthropomorphic chest phantom. *Eur Radiol* 9:1826–1834
22. Beute GH, Flynn MJ, Eyler WR, Samei E, Spizarny DL, Zylak CJ (1998) Chest radiographic image quality: comparison of asymmetric screen-film, digital storage phosphor, and digital selenium drum systems—preliminary study. *Radiographics* 18:745–754
23. Borasi G, Nitrosi A, Ferrari P, Tassoni D (2003) On site evaluation of three flat panel detectors for digital radiography. *Med Phys* 30:1719–1731
24. Samei E (2003) Image quality in two phosphor-based flat panel digital radiographic detectors. *Med Phys* 30:1747–1757
25. Granfors PR, Aufrichtig R (2000) Performance of a 41×41-cm<sup>2</sup> amorphous silicon flat panel x-ray detector for radiographic imaging applications. *Med Phys* 27:1324–1331
26. Volk M, Hamer OW, Feuerbach S, Strotzer M (2004) Dose reduction in skeletal and chest radiography using a large-area flat-panel detector based on amorphous silicon and thallium-doped cesium iodide: technical background, basic image quality parameters, and review of the literature. *Eur Radiol* 14:827–834
27. Bath M, Sund P, Mansson LG (2002) Evaluation of the imaging properties of two generations of a CCD-based system for digital chest radiography. *Med Phys* 29:2286–2297
28. Herrmann KA, Bonél H, Stäbler A et al (2002) Chest imaging with flat-panel detector at low and standard doses: comparison with storage phosphor technology in normal patients. *Eur Radiol* 12:385–390
29. Bacher K, Smeets P, Bonnarens K, De Hauwere A, Verstraete K, Thierens H (2003) Dose reduction in patients undergoing chest imaging: digital amorphous silicon flat-panel detector radiography versus conventional film-screen radiography and phosphor-based computed radiography. *Am J Roentgenol* 181:923–929
30. Goo JM, Im J-G, Lee HJ et al (2002) Detection of simulated chest lesions by using soft-copy reading: comparison of an amorphous silicon flat-panel detector system and a storage-phosphor system. *Radiology* 224:242–246
31. Aufrichtig R (1999) Comparison of low contrast detectability between a digital amorphous silicon and a screen-film based imaging system for thoracic radiography. *Med Phys* 26:1349–1358
32. Sund P, Bath M, Kheddache S, Mansson LG (2004) Comparison of visual grading analysis and determination of detective quantum efficiency for evaluating system performance in digital chest radiography. *Eur Radiol* 14:48–58
33. Burgess AE, Jacobson FL, Judy PF (2001) Human observer detection experiments with mammograms and power-law noise. *Med Phys* 28:419–437